



HAL
open science

High-resolution photoreceptor imaging analysis of patients with autosomal dominant retinitis pigmentosa (adRP) caused by HK1 mutation

Daiki Kubota, Kaori Matsumoto, Mika Hayashi, Noriko Oishi, Kiyoko Gocho, Kunihiro Yamaki, Shinichiro Kobayakawa, Tsutomu Igarashi, Hiroshi Takahashi, Shuhei Kameya

► **To cite this version:**

Daiki Kubota, Kaori Matsumoto, Mika Hayashi, Noriko Oishi, Kiyoko Gocho, et al.. High-resolution photoreceptor imaging analysis of patients with autosomal dominant retinitis pigmentosa (adRP) caused by HK1 mutation. *Ophthalmic Genetics*, 2020, pp.1-10. 10.1080/13816810.2020.1810284 . hal-02935407

HAL Id: hal-02935407

<https://hal.sorbonne-universite.fr/hal-02935407v1>

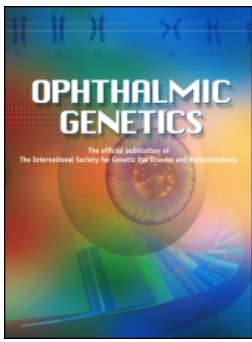
Submitted on 10 Sep 2020

HAL is a multi-disciplinary open access archive for the deposit and dissemination of scientific research documents, whether they are published or not. The documents may come from teaching and research institutions in France or abroad, or from public or private research centers.

L'archive ouverte pluridisciplinaire **HAL**, est destinée au dépôt et à la diffusion de documents scientifiques de niveau recherche, publiés ou non, émanant des établissements d'enseignement et de recherche français ou étrangers, des laboratoires publics ou privés.



Distributed under a Creative Commons Attribution - NonCommercial 4.0 International License



High-resolution photoreceptor imaging analysis of patients with autosomal dominant retinitis pigmentosa (adRP) caused by *HK1* mutation

Daiki Kubota , Kaori Matsumoto , Mika Hayashi , Noriko Oishi , Kiyoko Gocho , Kunihiro Yamaki , Shinichiro Kobayakawa , Tsutomu Igarashi , Hiroshi Takahashi & Shuhei Kameya

To cite this article: Daiki Kubota , Kaori Matsumoto , Mika Hayashi , Noriko Oishi , Kiyoko Gocho , Kunihiro Yamaki , Shinichiro Kobayakawa , Tsutomu Igarashi , Hiroshi Takahashi & Shuhei Kameya (2020): High-resolution photoreceptor imaging analysis of patients with autosomal dominant retinitis pigmentosa (adRP) caused by *HK1* mutation, *Ophthalmic Genetics*, DOI: [10.1080/13816810.2020.1810284](https://doi.org/10.1080/13816810.2020.1810284)

To link to this article: <https://doi.org/10.1080/13816810.2020.1810284>



© 2020 The Author(s). Published with license by Taylor & Francis Group, LLC.



[View supplementary material](#)



Published online: 20 Aug 2020.



[Submit your article to this journal](#)



Article views: 183



[View related articles](#)



[View Crossmark data](#)

High-resolution photoreceptor imaging analysis of patients with autosomal dominant retinitis pigmentosa (adRP) caused by *HK1* mutation

Daiki Kubota^{a+}, Kaori Matsumoto^{a,b+}, Mika Hayashi^{a+}, Noriko Oishi^a, Kiyoko Gocho^{a,c}, Kunihiko Yamaki^a, Shinichiro Kobayakawa^d, Tsutomu Igarashi^b, Hiroshi Takahashi^b, and Shuhei Kameya^a

^aDepartment of Ophthalmology, Nippon Medical School Chiba Hokusoh Hospital, Inzai, Chiba, Japan; ^bDepartment of Ophthalmology, Nippon Medical School, Tokyo, Japan; ^cClinical Investigation Center 1423, Inserm and Quinze-Vingts National Ophthalmology Hospital, Paris, France; ^dDepartment of Ophthalmology, Nippon Medical School Musashikosugi Hospital, Kawasaki-city, Japan

ABSTRACT

Purpose: The hexokinase 1 (*HK1*) gene encodes one of the four human hexokinases that play essential roles in glucose metabolism. Recently, several cases of E847K mutation in the *HK1* gene were reported to cause inherited retinal dystrophy. The purpose of this study was to identify the phenotypical characteristics of patients with a recurrent E847K mutation in the *HK1* gene.

Methods: Three generations of one family with autosomal dominant retinitis pigmentosa were examined. Whole exome sequencing was performed on the DNA. Fundus imaging by an adaptive optics fundus camera was used to obtain high-resolution photoreceptor images.

Results: Fundus examination of the proband showed degeneration of the mid-peripheral retina, and SD-OCT images showed an absence of the ellipsoid zone (EZ) and interdigitation zone (IZ) in the parafovea and more peripherally. SD-OCT images of the mother of the proband showed an absence of the EZ and IZ, and fundus autofluorescence images showed hypo-autofluorescence surrounding the macular region. One daughter of the proband had only mild night blindness, however, the density of the cone photoreceptors was reduced in the parafoveal region. Whole exome sequencing identified a heterozygous variant, E847K, in the *HK1* gene. This variant was found to co-segregate with the disease in three family members.

Conclusions: Although the systemic phenotypes were found to be associated with the *HK1* mutations, only the E847K mutation can cause a non-syndromic photoreceptor degeneration. Our study strengthened the hypothesis that the amino acid E847 might play a critical role in the maintenance of the morphology and function of the photoreceptors.

ARTICLE HISTORY

Received June 02, 2020

Revised July 11, 2020

Accepted August 09, 2020

KEYWORDS

HK1; adaptive optics; whole exome sequencing; adRP

Introduction

The *hexokinase 1* (*HK1*; OMIM 14260) gene encodes one of the four human hexokinases that play essential roles in glucose metabolism (1–3). Hexokinase catalyzes the first step in glucose metabolism using ATP for the phosphorylation of glucose to glucose-6-phosphate. Four different forms of hexokinase, HK1, HK2, HK3, and HK4 that are encoded by different genes, are present in mammalian tissues (3). Among these, HK1 is the most ubiquitously expressed and is the predominant hexokinase in the brain, erythrocytes, lymphocytes, and fibroblasts (1). A proteomic study of rats found that HK1 and HK2 are expressed in the retina (4). HK1 was found to be strongly expressed in the photoreceptor inner segment and in the outer plexiform layer, inner nuclear layer, inner plexiform layer, and ganglion cell layer (4).


Thus far, four phenotypes that are associated with *HK1* mutations have been listed in the OMIM database (5). They are nonspherocytic hemolytic anemia (NSHA) due to hexokinase deficiency (OMIM; 235700), Russe type of hereditary motor and sensory neuropathy (HMSNR, OMIM; 605285),

retinitis pigmentosa 79 (RP79, OMIM; 617460), and neuro-developmental disorder with visual defects and brain anomalies (NEDVIBA, OMIM; 618547). NSHA, due to hexokinase deficiency, and the Russe type of HMSNR are autosomal recessive inheritance disorders that are caused by homozygous or compound heterozygous loss-of function mutations of the *HK1* gene (6–8). On the other hand, five families of autosomal dominant retinitis pigmentosa (adRP; RP79) were reported by Sullivan et al. who reported on a heterozygous missense Glu847Lys (E847K) mutation in the *HK1* gene that segregated fully with the disease in each family (9). None of the patients had any extraocular manifestations, and none had any systemic abnormalities in glycolysis (9). Later, several groups reported similar non-syndromic autosomal dominant retinitis pigmentosa or allied diseases with the same heterozygous E847K mutation in the *HK1* gene (10–13). Most recently, seven patients from six unrelated families with NEDVIBA were reported by Okur et al. They identified four different de novo heterozygous missense mutations in the *HK1* gene in these patients (14). They also reported that

CONTACT Shuhei Kameya,  shuheik@nms.ac.jp, Department of Ophthalmology, Nippon Medical School Chiba Hokusoh Hospital, Inzai, Chiba 270-1694, Japan

⁺These authors contributed equally to this study.

All persons designated as authors had qualified ICJME requirements for authorship.

 Supplementary data for this article can be accessed on the [journal website](#).

© 2020 The Author(s). Published with license by Taylor & Francis Group, LLC.

This is an Open Access article distributed under the terms of the Creative Commons Attribution-NonCommercial License (<http://creativecommons.org/licenses/by-nc/4.0/>), which permits unrestricted non-commercial use, distribution, and reproduction in any medium, provided the original work is properly cited.

these patients were syndromic, and several cases had a combination of retinitis pigmentosa and optic atrophy. However, the inheritance pattern and detailed ophthalmic findings were uncertain because a pedigree analysis and fundus images were not presented (14).

The purpose of this study was to determine the phenotypic characteristics of the members of a Japanese family with a recurrent E847K mutation in the *HK1* gene. To accomplish this, the family members underwent comprehensive ocular examinations including high-resolution retinal imaging by an adaptive optics fundus camera.

Methods

The procedures used in this study conformed to the tenets of the Declaration of Helsinki, and they were approved by the Institutional Review Board of the Nippon Medical School. A signed written informed consent was obtained from the proband and her daughters after the nature and possible consequences of the study were explained.

The ophthalmological examinations included measurements of the best-corrected visual acuity (BCVA) and refractive error (spherical equivalent), slit-lamp biomicroscopy, ophthalmoscopy, Goldman kinetic perimetry, fundus photography (CLARUS, Carl Zeiss Meditec), fundus autofluorescence imaging with short-wavelength excitation (FAF; CLARUS, 500–585 nm, Carl Zeiss Meditec and TRC-NW8Fplus retinal camera, 488 nm, TOPCON, Tokyo, Japan), spectral domain optical coherence tomography (SD-OCT; Cirrus HD-OCT, Carl Zeiss Meditec), full-field electroretinography (ERG), and multifocal ERGs (mfERGs). The ERGs were recorded using the extended testing protocol conforming to the International Society for Clinical Electrophysiology of Vision protocol (15). The ERGs were elicited and recorded with a contact lens with a built-in LED electrode (LE4000, TOMEY, JAPAN). ERG responses of patients were compared to controls (9 men and 15 women, median age 44.5 ± 19.8 years). The mfERGs were recorded with a commercial mfERG system (LE4100, TOMEY, JAPAN).

Adaptive optics (AO) image analysis

High-resolution retinal images were acquired with the Adaptive Optics Retina Camera (rtx1™, Imagine Eyes, Orsay, France), at temporal eccentricities of 2 to 8 degrees. The AO images from one retina were stitched together by an automated image editing software (ImageJ, National Institute of Health, Bethesda, MD).

We used a reported protocol to obtain the peak density of the cones for the measurement of the cone density based on a technique described in detail by Feng et al. (16,17). The cone densities of Patients II-3, III-1, and III-2 were compared to 34 healthy individuals (27 men and 7 women, mean age 37.4 ± 9.1 years, range 24 to 55 years) (16). Color-coded Voronoi diagrams of the cone density analysis were performed with the built-in software in the rtx1 (AO detect, Imagine Eyes, Orsay, France).

Genetic analyses

Blood samples were collected from the proband (II-3) and her daughters (III-1, III-2), and genomic DNA was isolated from the peripheral white blood cells using a blood DNA isolation kit (NucleoSpin Blood XL; Macherey Nagel, Germany). Exome sequencing (Macrogen Japan) and targeted sequence analysis were done. Paired-end sequence library construction and exome capturing were performed by the Agilent Bravo automated liquid-handling platform with the Agilent SureSelect Human v6 kit (Agilent Technologies, Santa Clara, CA). Enriched libraries were sequenced with the Illumina NovaSeq6000 sequencer (San Diego, CA). The reads were aligned to the UCSC Hg38 reference sequence with the Burrows-Wheeler Aligner software (18). Duplicated reads were removed by Picard MarkDuplicates module, and mapped reads around insertion-deletion polymorphisms (INDELs) were realigned by the Genome Analysis Toolkit (GATK) (19). Base-quality scoring was recalibrated by GATK. Mutation calling was performed with the GATK Unified Genotyper module. The called single-nucleotide variants (SNVs) and INDELs were annotated by the snpEff software (snpEff score; “HIGH,” “MODERATE,” or “LOW”) (20). All called SNVs and INDELs of the 271 genes registered as retinal disease-causing genes on the RetNet database were selected for further analysis (<https://sph.uth.edu/retnet/home.htm>). The identified variants were filtered with allele frequency (less than 1%) of the Human Genetic Variation Database (HGVD; <http://www.genome.med.kyoto-u.ac.jp/SnpDB/about.htm>) which is specific for the Japanese population. Depth and coverage for the targeted areas were made visible and confirmed with the integrative Genomics Viewer (<http://www.broadinstitute.org/igv/>). All identified variants were analyzed using varsome (varsome.com). The allelic frequency of all of the variants was estimated in reference to three data bases; HGVD, iJGVD, and gnomAD Browser. Pathogenicity classification of all detected variants was performed based on the guidelines of the American College of Medical Genetics and Genomics (ACMG) (21). Together with the clinical findings of the affected subjects, the mode of inheritance in the pedigree, as well as cosegregation, disease-causing variants were determined from the called variants in the retinal disease-associated genes. The *HK1* variants identified by exome sequencing and targeted analysis were further confirmed by direct sequencing of family members. The identified regions were amplified by polymerase chain reaction (PCR) using primers synthesized by Greiner Bio-One (Tokyo, JAPAN). The PCR products were purified (ExoSAP-IT; USB Corp., USA) and were used as the template for sequencing. Both strands were sequenced on an automated sequencer (Bio Matrix Research; Chiba, JAPAN).

Results

Clinical findings

A 49-year-old woman (II-3; proband) was informed of fundus abnormalities during a general health checkup and visited our hospital. She reported that she had a gradual decrease of vision and increase of night blindness. Our examinations showed no obvious cataracts and her decimal BCVA was 1.0 in both eyes.

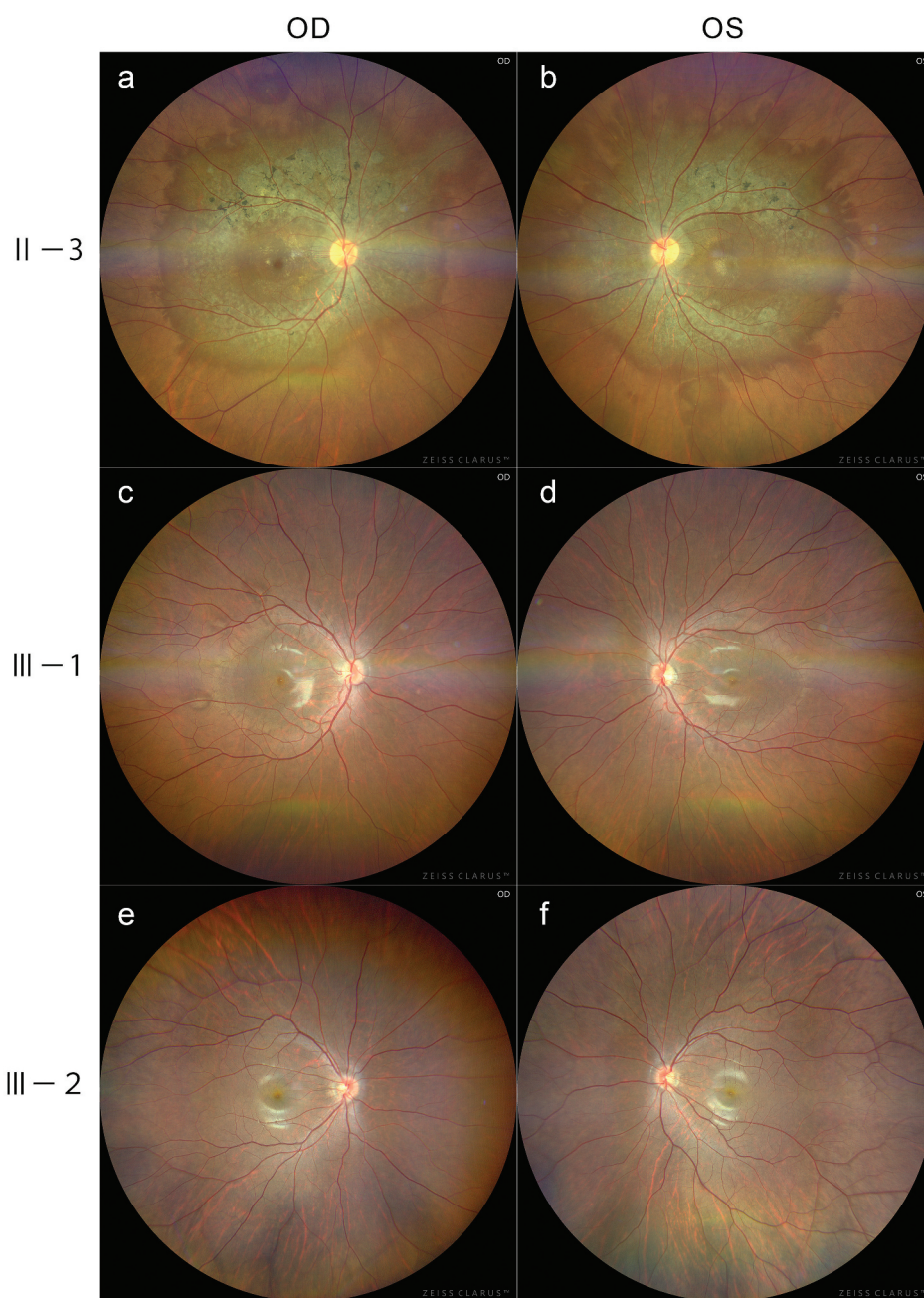


Figure 1. Ultra-widefield fundus photographs of family members with autosomal dominant retinitis pigmentosa (adRP). Images of patients II-3 (A, B), III-1 (C, D), and III-2 (E, F) are shown. Fundus photographs of II-3 show chorioretinal atrophy around the retinal vascular arcade with granular macular RPE mottling. Fundus photographs of III-1 show slight alterations of the macular ring reflex in both eyes and spots of RPE color changes outside the retinal vascular arcades of the right eye. Fundus photographs of III-2 show no abnormalities in both eyes.

However, she had symmetrical fundus abnormalities consisting of chorioretinal atrophy around the retinal vascular arcade. She stated that her mother (I-2) and grandmother had been diagnosed with retinitis pigmentosa. Her mother had visited our hospital only once when she was 80-years-old, and her medical record revealed that her decimal BCVA was 0.03 in the right eye and 0.05 in the left eye. The proband had two daughters, and their examination revealed that one of her daughters (III-1; 20 years) had fundus abnormalities. The decimal BCVA of this daughter was 1.0 in both eyes, and she reported only mild night blindness.

Fundus examination of II-3 showed symmetrical chorioretinal atrophy around the retinal vascular arcade with granular macular RPE mottling [Figure 1A, B](#). Fundus examination of III-1 showed slight disturbances of macular ring reflex in both eyes, and spots of RPE color changes outside the retinal vascular arcades in the right eye. Patient III-2 had no abnormalities in either eye [Figure 1\(C-F\)](#).

The FAF images found in the medical records of I-2 showed profound hypo-autofluorescence surrounding the macular region of both eyes [Figure 2\(A, B\)](#). The choroidal vessels were visible through the hypo-autofluorescent areas [Figure 2\(A, B\)](#). The FAF

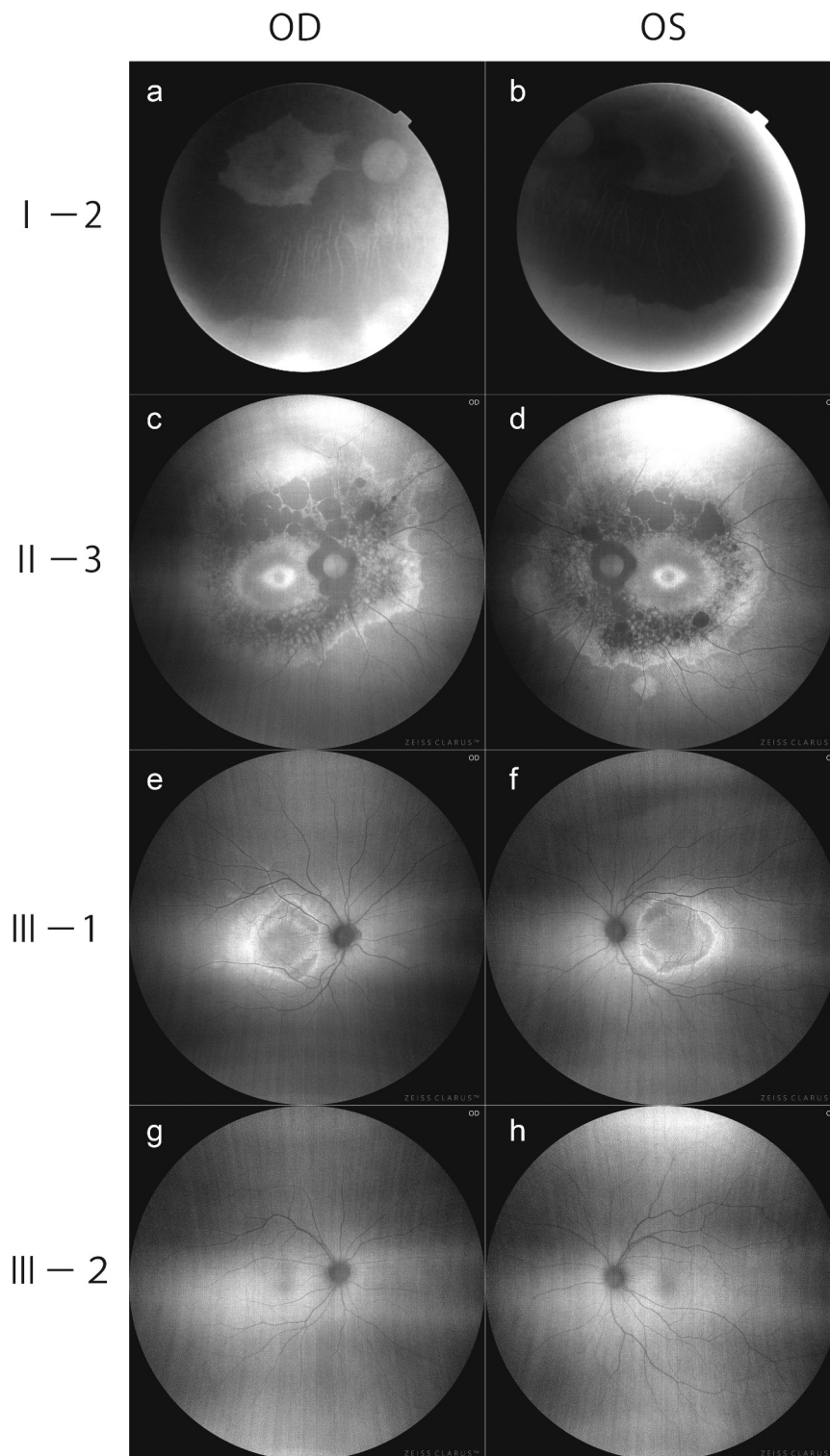


Figure 2. Fundus autofluorescence (FAF) images of family members with adRP. FAF Images of I-2 (A, B), II-3 (C, D), III-1 (E, F), and III-2 (G, H) are shown. FAF of I-2 were the conventional 45 degrees of field of view images. FAF of II-3 (C, D), III-1 (E, F), and III-2 were 133 degrees of widefield angle of view. FAFs of I-2 show severe hypo-autofluorescence surrounding the macular region in both eyes. Choroidal vessels can be seen through the hypo-autofluorescent area of I-2. FAFs of II-3 show cobblestone hypo-autofluorescent regions around the retinal vascular arcade. The FAF images of II-3 also show a new contrast between the possible preserved foveal and parafoveal autofluorescence and the hypo-autofluorescent lesion in the pericentral and near midperipheral retina. FAFs of III-2 show a hyper-autofluorescent ring surrounding a hypo-autofluorescent area in the parafoveal area of both eyes. Spots of hyper-autofluorescence can be seen in the right eye of III-1 corresponding to the RPE abnormalities seen in the color photographs. The peripheral area other than these spots are normal appearing in both eyes of III-1. FAFs of III-2 show no abnormalities in both eyes.

images of II-3 showed a cobblestone hypo-autofluorescent region around the retinal vascular arcade [Figure 2\(C, D\)](#). The FAF images of II-3 also showed a new contrast between the possible preserved foveal and parafoveal autofluorescence and the hypo-

autofluorescent lesion in the pericentral and near midperipheral retina. FAFs of III-1 showed a hyper-autofluorescence ring surrounding a hypo-autofluorescent area in the parafoveal region of both eyes [Figure 2E, F](#). Spots of hyper-autofluorescence were

observed in the right eye of III-1 corresponding to the RPE abnormalities found in the color photographs Figure 2(E, F). The peripheral area other than these spots were normal in appearance in both eyes of III-1 Figure 2(E, F). FAFs of III-2 showed no abnormalities in both eyes Figure 2(G, H). The SD-OCT images of the eyes of I-2 showed an absence of the EZ and IZ and thinning of the outer nuclear layer (ONL) throughout the 6 mm images Figure 3(A, B). The SD-OCT images of the eyes of II-3 showed locally preserved EZ and IZ at the foveola although there was an absence of the EZ and IZ and thinning of the ONL from the parafovea and more peripherally in the central retinal scan Figure 3(C, D). Cystoid macular edema was found on the nasal side of the inner nuclear layer of both eyes of II-3 Figure 3(C, D). The SD-OCT images of the eyes of III-1 showed clearly distinguishable EZ and IZ in the fovea, however, the EZ and IZ were discontinuous in the parafoveal area Figure 3(E, F). The ONL was also thinner in the parafoveal area of both eyes of III-1 Figure 3(E, F). The SD-

OCT images of III-2 showed no abnormalities with intact EZ and IZ Figure 3(G, H).

The visual fields were full and ring scotomas were detected in both eyes of II-3 with Goldmann kinetic visual field test Figure 4(A, B). Relative pericentral ring scotoma was detected with the I-4 target. The visual fields test of III-1 showed no abnormalities in both eyes Figure 4(C, D).

Full-field ERGs showed that the b-wave amplitude of the dark-adapted 0.01 and the a- and b-wave amplitudes of dark-adapted 3.0 were slightly reduced in both eyes in II-3 Figure 5(A-D). The implicit time of the light-adapted 3.0 flicker ERGs was slightly prolonged in both eyes of II-3 Figure 5D. The oscillatory potentials of the dark-adapted 3.0 were also reduced in both eyes of II-3 Figure 5B. The responses of III-2 were normal in both eyes Figure 5(E-H). The amplitudes of the mfERGs in the parafoveal area were mildly reduced, although that in foveal center were preserved in II-3 Figure 6(A, B, E, F).

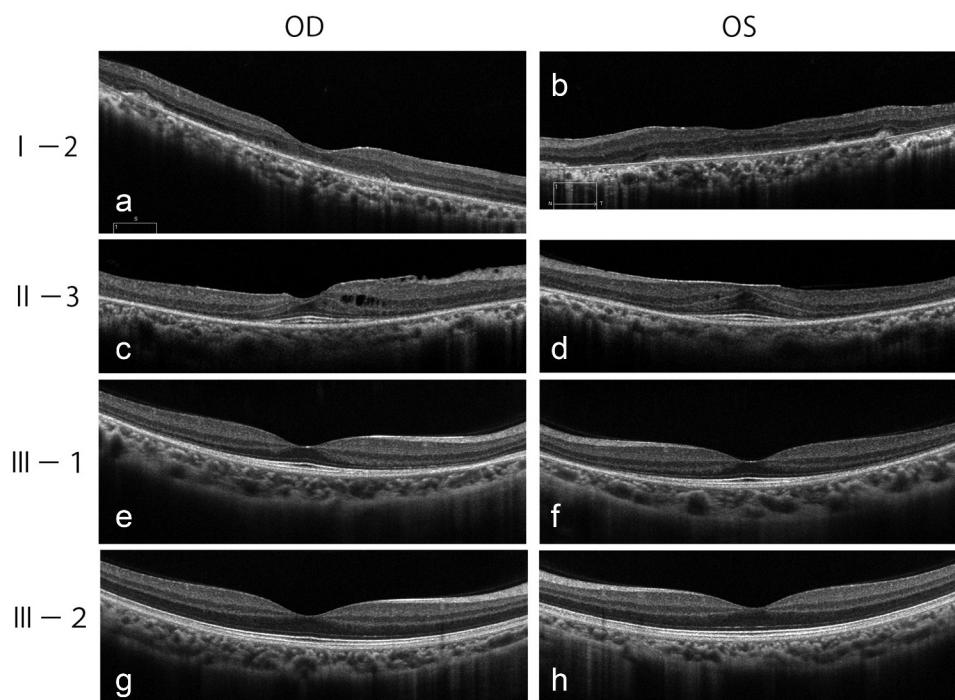


Figure 3. Spectral domain optical coherence tomographic (SD-OCT) images of family members with adRP. SD-OCT images of I-2 (A, B), II-3 (C, D), III-1 (E, F), and III-2 (G, H) are shown. The SD-OCT images of the eyes of I-2 show an absence of the ellipsoid zone (EZ) and interdigitation zones (IZ) and thinning of the outer nuclear layer (ONL) throughout the 6 mm images. The SD-OCT images of the eyes of II-3 show locally intact EZs and IZs at the foveola, although the absence of the EZs and IZs and thinning of the ONL from the parafovea and beyond can be seen. Cystoid macular edema can be seen on the nasal side of the inner nuclear layer in both eyes of II-3. The SD-OCT images of the eyes of III-1 show clearly distinguishable EZs and IZs in the fovea, however the EZs and IZs are discontinuous in the parafoveal area. The ONL is also thinner in the parafoveal area in both eyes of III-1. The SD-OCT images of III-2 show no abnormalities with intact EZs and IZs.

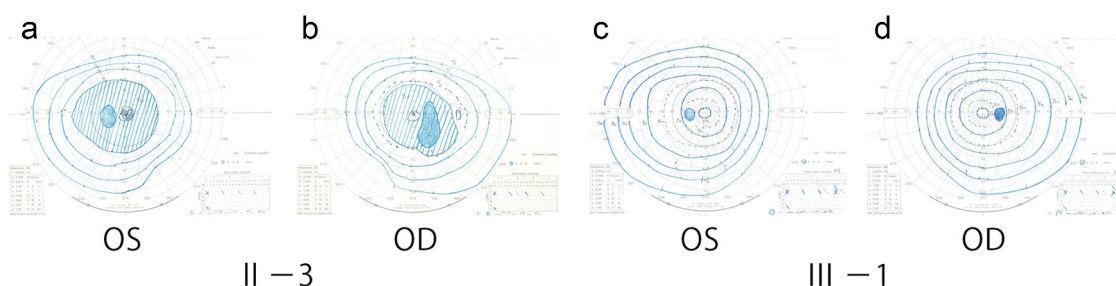


Figure 4. Results of Goldmann kinetic visual field test of family members. Results of Goldmann kinetic visual field test of left eye (A, C) and right eye (B, D) of the patient II-3 (A, B) and III-1 (C, D) are shown. The visual fields are full and ring scotomas can be seen in both eyes of II-3. Relative pericentral ring scotoma is detected with the I-4 target. Results of III-1 show no abnormalities in both eyes.

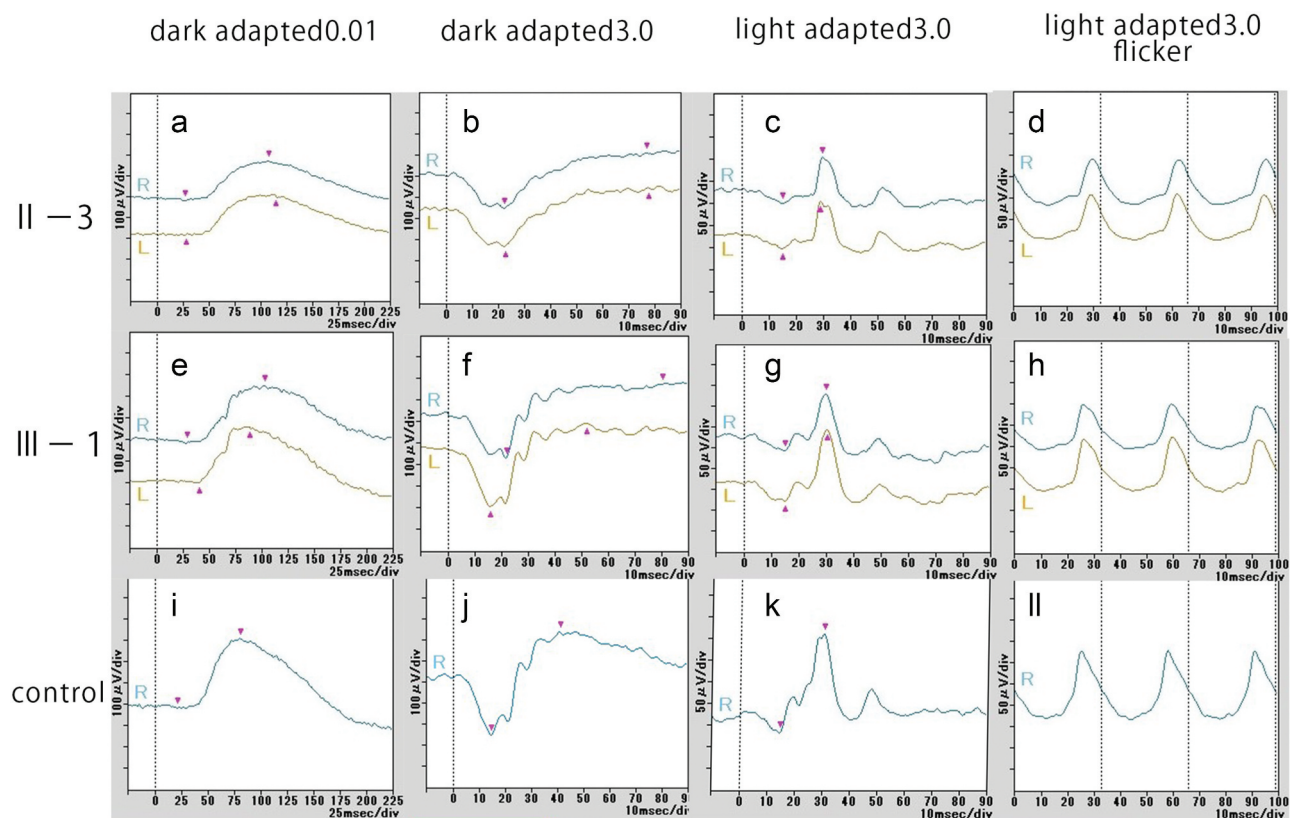


Figure 5. Full-field electroretinograms (ERGs) of family members with adRP. Full-field ERGs recorded from II-3 (A-D), III-1 (E-H), and normal control (I-L) are shown. The dark-adapted 0.01 (A, E, I), dark-adapted 3.0 (B, F, J), light-adapted 3.0 (C, G, K), and light-adapted 3.0 flicker ERGs (D, H, L) are shown. The b-wave amplitude of dark-adapted 0.01 and the a- and b-wave amplitude of dark-adapted 3.0 show a slight reduction in both eyes in II-3. The implicit times of light-adapted 3.0 flicker ERGs are slightly prolonged in both eyes in II-3. The oscillatory potentials of dark-adapted 3.0 are also reduced in both eyes in II-3. The results of all the responses in III-2 showed no abnormality in both eyes.

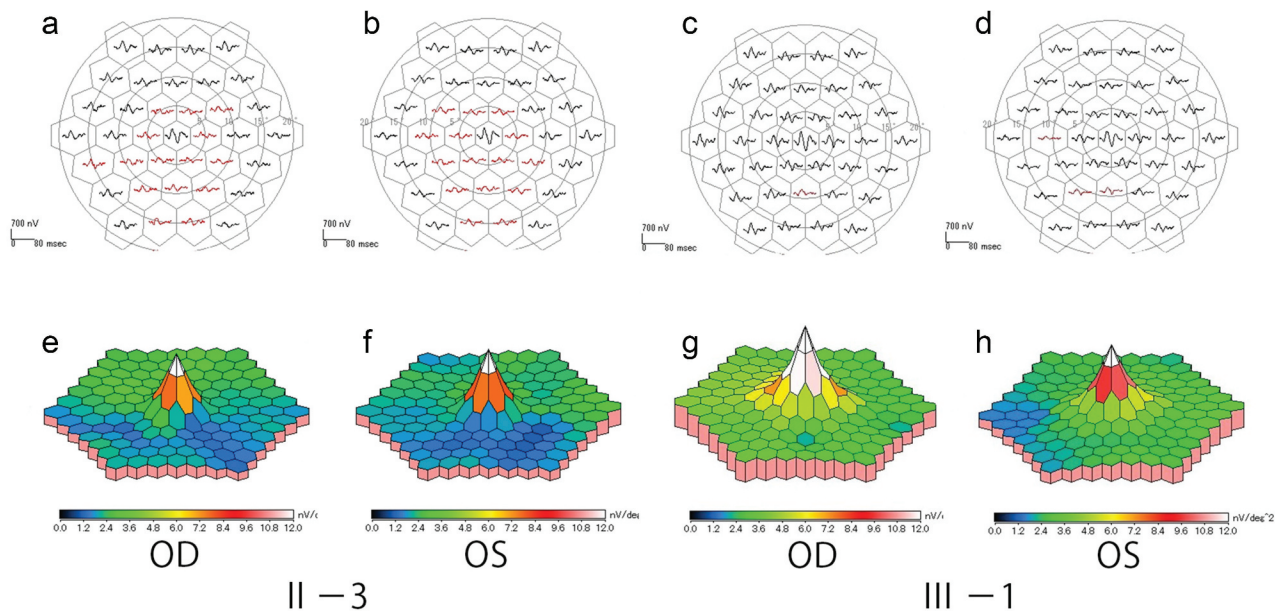


Figure 6. Multifocal ERGs (mfERGs) of family members. The mfERGs and topographic map of patients II-3 (A, B, E, F) and III-1 (C, D, G, H) are shown. The amplitudes of the mfERGs in the parafoveal area are slightly reduced, although those in the foveal center are preserved in II-3. The amplitudes of the mfERGs in the parafoveal area are partially and slightly reduced in III-1.

The amplitudes of the mfERGs in the parafoveal area were partially and slightly reduced in III-1 **Figure 6(C, D, G, H)**. No systemic abnormalities were found in II-3, III-1, and III-2.

Molecular genetic analyses

We identified a heterozygous variant, c.2539 G > A, p.E847K in the *HK1* gene by WES in the DNA samples of II-3 and III-1 **Figure 7(A- D)**. The variant was not observed in the DNA samples of III-2. The *HK1* variant was the only gene with HIGH score of snpEff and less than 0.1% of allelic frequency in the RetNet genes. This variant was verified by Sanger sequencing, and it co-segregated with the disease in three members of the family **Figure 7(C, D)**. The allele was not observed in the Japanese specific (HGVD, iJGVD) and gnomAD databases.

Analyses of high-resolution images obtained by adaptive optics (AO) fundus camera

Regular cones were not observed throughout the posterior pole in the AO images of II-3 **Figure 8(A- D)**. The images of III-1 showed a reduction of the cone densities in the posterior pole **Figure 8(B- E)**. The AO images of III-2, who did not harbor the variant p.E847K in the *HK1*, showed a regular cone mosaic and normal densities **Figure 8(C- F)**. The cone densities from patients II-3, III-1, and III-2 were compared to that of the normal control

eyes. The cone densities of patient II-3 were uncountable throughout 2 to 5 degrees **Figure 8D**. The cone densities of patient III-1 were lower by more than 2 standard deviation from that of the normal control throughout the 2- to 5-degree field **Figure 8D**. The cone densities of patient III-2 were within 2 standard deviation of that of the normal control throughout the 2- to 5-degree field **Figure 8D**. Color-coded Voronoi diagrams that show the cone densities of III-1 and III-2 at 2 degrees angular eccentricity are presented in **Figures 8E and 8F**. Note that the images at sites closer than 2 degrees to the foveal center of III-2 showed a very high density of cones that could not be discriminated **Figure 8C**. This was because the size of cones becomes less than the discriminable level of the AO fundus camera (<2 micrometer) as was true for normal control. However, the image of III-1 had discriminable cones even less than 1 degree from the fovea center because of the reduced cone density **Figure 8B**.

Discussion

A recurrent heterozygous E847K mutation in *HK1* was found in two Japanese patients from a family with adRP. Fundus, FAF, and OCT imaging revealed that the areas of photoreceptor degeneration were mainly in the parafovea to mid-peripheral region. Multifocal ERGs, Goldmann visual field tests, and visual acuity measurements revealed that the fovea was still functioning until the age of the late 40 years. Full-field ERGs revealed that all components of the full-field ERGs were almost normal at age of

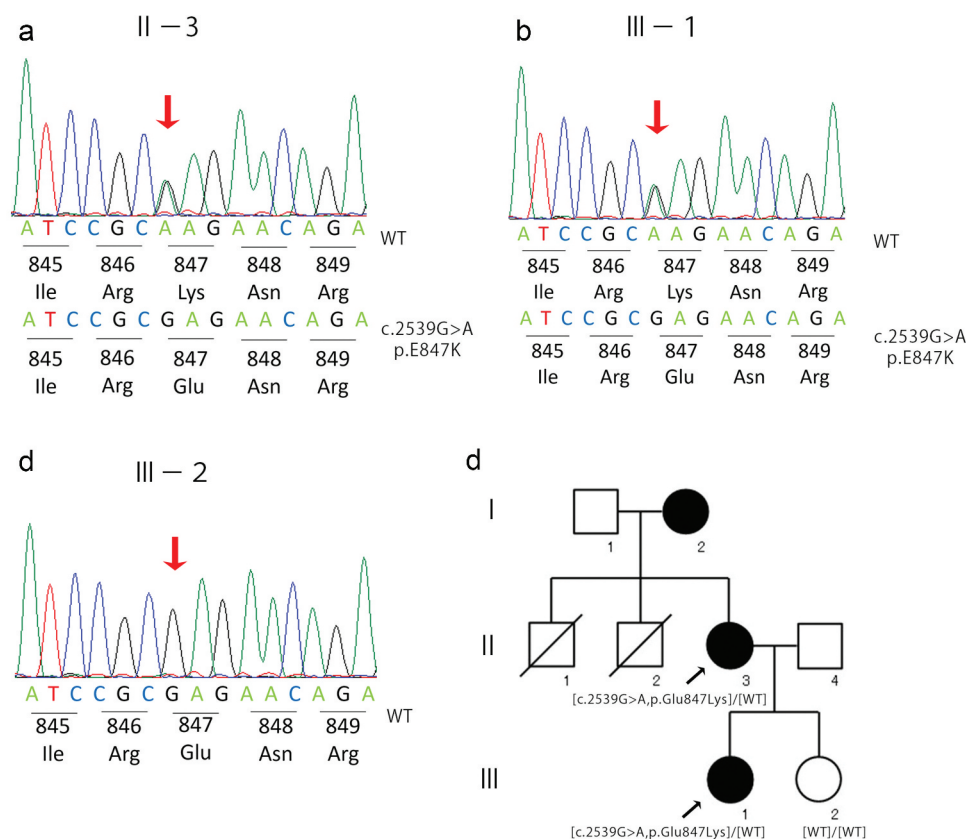


Figure 7. Molecular genetic findings and segregation scheme. Sequence chromatograms of *HK1* variants from II-3 (A) III-1 (B) and III-2 (C) are shown. Pedigree charts for the segregation analysis are shown (D). Red arrow indicates the position of the mutation. II-3 and III-2 had [c.2539 G > A, p.E847K] variant. The affected female patients are represented with the solid circle and unaffected family members are represented by white icons. The slash symbol indicates deceased individuals. The generation is numbered on the left. Segregation analysis of a variant of *HK1* in the family show co-segregation of the disease-causing variant and phenotypes.

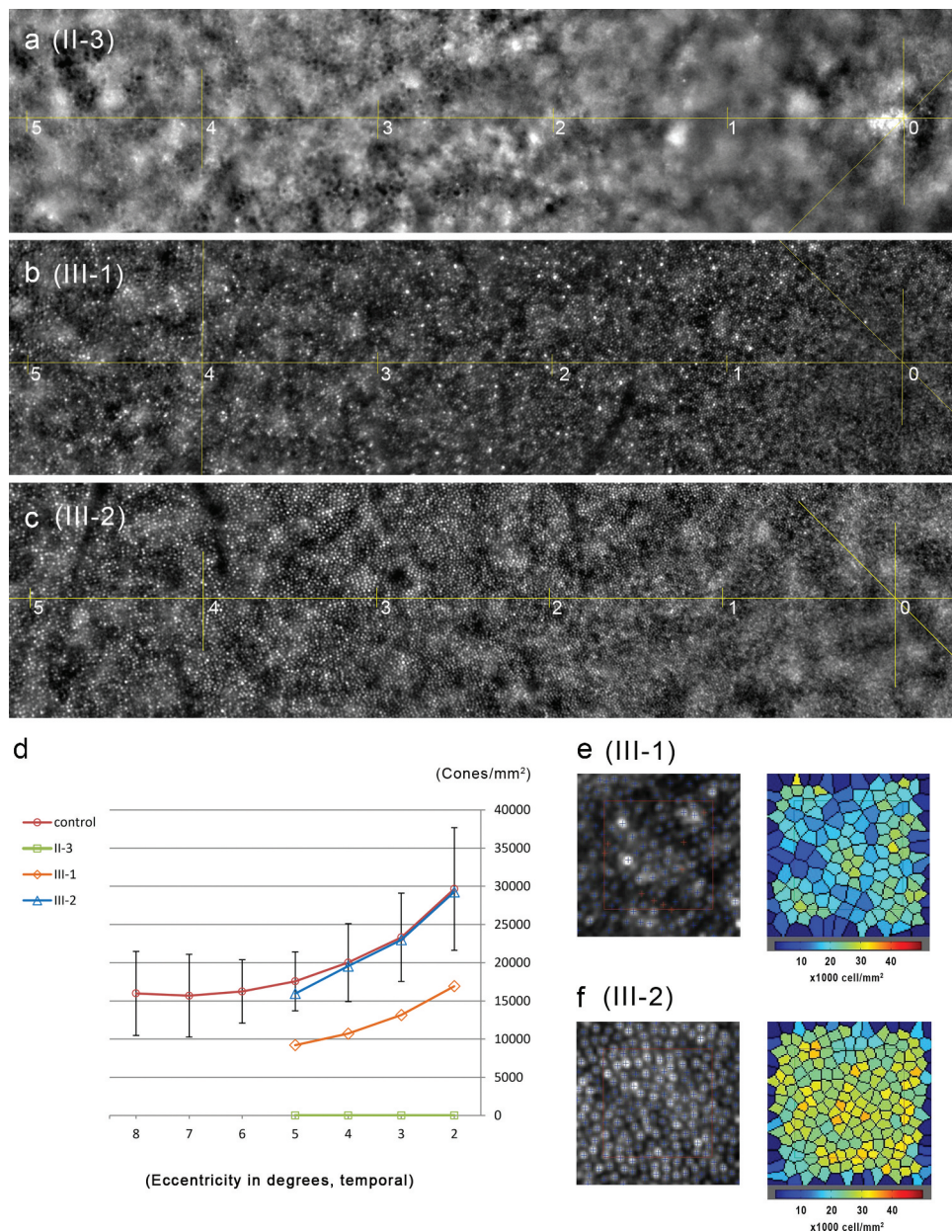


Figure 8. Adaptive optics images and cone densities of patients. AO images of Patients II-3 (A), III-1 (B), and III-2 (C) are shown. The temporal retina at angular eccentricities of 0 degrees (foveal center) to 5 degrees are shown. Yellow crosses with diagonal line indicate foveal center. Horizontal lines are drawn from foveal center to temporal retina. Numbers in figures indicate angular eccentricities of nearby yellow crosses from foveal center. Regular cones are not observed throughout the posterior pole in the AO image of II-3. The image of III-1 shows reduced cone densities in the area as shown in D. Image of III-2, who does not harbor the variant p.E847K in the *HK1*, show regular cone mosaic and densities as shown in D. (D) Cone density from patients II-3, III-1 and III-2 are compared with normal control. Cone densities of patient III-1 are lower by more than 2 standard deviation from that of the normal control from 2 to 5 degrees. Cone densities of the patient III-2 are within 2 standard deviation of that of the normal control throughout 2 to 5 degrees. Color-coded Voronoi diagrams that show the cone densities of III-1 and III-2 at 2 degrees angular eccentricity are presented in Figures 8E and 8 F. Cone density of patient II-3 are not countable throughout 2 to 5 degrees. Note that cone images at closer than 2 degrees to the foveal center should be uncountable because of the high cone density in normal control same as case of III-2 (Figure 8 C). This is because the size of the cones become less than the discriminable limit of AO fundus camera (< 2 micrometer). However, the image of III-1 showed discriminable cones even less than 1 degrees because of the reduced cone density (Figure 8D).

20 years, and a mild reduction was observed in the late 40s. However, high-resolution retinal imaging by AO revealed that the cone photoreceptor densities were significantly reduced in the parafoveal area at the age of 20 years. Fundus examinations showed only slight abnormalities without functional visual defects at this age.

The clinical phenotypes of 10 Caucasian and 2 Asian families with non-syndromic adRP or adCACD caused by an E847K

mutation of the *HK1* have been reported in Table 1 (9–13). A relatively good visual acuity and mild photoreceptor degeneration in the mid-peripheral area were common features in most of these patients. None of the patients with the E847K mutation had optic disc atrophy. There is also a report describing patients with syndromic RP and/or optic atrophy caused by Gly414Glu, Ser445Leu, and Thr457Met mutations in the *HK1* gene (14). From these earlier findings and our data, we conclude that patients

Table 1. Genetic and clinical characteristics of previously reported ocular phenotypes with *HK1* variants.

HGVS.p	Inheritance	Syndromic or not	Ocular Phenotype	Number of family / Ethnicity	Year	Reference
p.Gly414Glu	n.a.	syndromic	Retinitis pigmentosa	1/n.a.	2019	Okur V, et al. (14)
p.Ser445Leu	n.a.	syndromic	Retinitis pigmentosa, and Optic atrophy	2/n.a.	2019	Okur V, et al. (14)
p.Thr457Met	n.a.	syndromic	Optic atrophy	3/n.a.	2019	Okur V, et al. (14)
p.Glu847Lys	AD	not	Retinitis pigmentosa or CACD	5/Americans or Europeans	2014	Sullivan LS, et al (9)
p.Glu847Lys	AD	not	Retinitis pigmentosa	1/Caucasian	2014	Wang F, et al. (10)
p.Glu847Lys	AD	not	Retinitis pigmentosa	3/Caucasian 1/Chinese	2017	Yuan Z, et al (11)
p.Glu847Lys	AD	not	Retinitis pigmentosa	1/Spanish	2018	Martin-Merida I, et al. (12)
p.Glu847Lys	AD	not	Retinitis pigmentosa	1/Japanese	2019	Sato S, et al. (13)

with E847K and other mutations are completely different from the point of view of systemic diseases. The molecular pathogenesis of E847K and other mutations should be different, although there are possibilities to explain the differences other than a molecular mechanism. Biochemical studies have shown that the E847K variant does not affect the hexokinase activity or stability of the *HK1* protein (10). It had been suggested that a gain-of-function of *HK1* by E847K mutations acquired pathogenicity for the retinopathy (12). Thus, amino acid E847 might play a critical role in the maintenance of the morphology and function of the photoreceptors.

There are limitations to this study. Although this is the first report to present a comprehensive ophthalmic analysis including high-resolution imaging of the photoreceptors in patients with the E847K mutation in the *HK1* gene, only two cases were studied in detail. A larger number of patients with this mutation are needed to allow us to determine more accurate relationships between the E847K mutations and photoreceptor degeneration and other manifestations.

In conclusion, our findings indicate that the functional visual defects are mild in patients with the E847K mutation in the *HK1* gene. The disease progression is slow, and symptoms begin in the late 40s, although a reduction in the cone photoreceptor density begins in the teenage years. Because the ophthalmological phenotypes of younger patients are mild, ophthalmologists should be very careful in evaluating the clinical findings in patients with these phenotypes. High-resolution retinal imaging analysis, such as that by AO and FAF analysis would be helpful in identifying patients with *HK1*-retinopathy caused by an E847K mutation.

Acknowledgments

We thank Professor Emeritus Duco Hamasaki of the Bascom Palmer Eye Institute, University of Miami School of Medicine, Miami, FL for discussions, and editing our manuscript.

Disclosure of interest

Spouse of Dr. Kiyoko Gocho is Co-founder and CEO of Imagine eyes. Other authors declare that they have no competing interests.

Funding

JSPS KAKENHI Grant Number: 19K09940 Japan Society for the Promotion of Science (JSPS).

Ethical approval

All procedures performed in studies involving human participants were in accordance with the ethical standards of the institutional research committee and with the 1964 Helsinki declaration and its later amendments or comparable ethical standards.

Informed consent

Informed consent was obtained from all individual participants included in the study.

References

- Katzen HM, Schimke RT. Multiple forms of hexokinase in the rat: tissue distribution, age dependency, and properties. *Proc Natl Acad Sci U S A.* 1965 Oct;54(4):1218–25. PMID: 5219826; PMCID: PMC219842. doi:10.1073/pnas.54.4.1218.
- Aleshin AE, Zeng C, Bourenkov GP, Bartunik HD, Fromm HJ, Honzatko RB. The mechanism of regulation of hexokinase: new insights from the crystal structure of recombinant human brain hexokinase complexed with glucose and glucose-6-phosphate. *Structure.* 1998 Jan 15;6(1):39–50. PMID: 9493266. doi:10.1016/s0969-2126(98)00006-9.
- Irwin DM, Tan H. Evolution of glucose utilization: glucokinase and glucokinase regulator protein. *Mol Phylogenet Evol.* 2014 Jan;70:195–203. Epub 2013 Sep 25. PMID: 24075984; PMCID: PMC3897444. doi:10.1016/j.ympev.2013.09.016
- Reidel B, Thompson JW, Farsiu S, Moseley MA, Skiba NP, Arshavsky VY. Proteomic profiling of a layered tissue reveals unique glycolytic specializations of photoreceptor cells. *Mol Cell Proteomics.* 2011 Mar;10(3):M110.002469. Epub 2010 Dec 20. PMID: 21173383; PMCID: PMC3047149. doi:10.1074/mcp.M110.002469.
- Online Mendelian Inheritance in Man, OMIM: www.omim.org. McKusick-nathans institute of genetic medicine, Johns Hopkins University (Baltimore, MD): United States. Available from: <https://omim.org/>.
- Rijksen G, Akkerman JW, van den Wall Bake AW, Hofstede DP, Staal GE. Generalized hexokinase deficiency in the blood cells of a patient with nonspherocytic hemolytic anemia. *Blood.* 1983 Jan;61(1):12–18. PMID: 6848140. doi:10.1182/blood.V61.1.12.12.
- van Wijk R, Rijksen G, Huizinga EG, Nieuwenhuis HK, van Solinge WW. HK Utrecht: missense mutation in the active site of human hexokinase associated with hexokinase deficiency and severe nonspherocytic hemolytic anemia. *Blood.* 2003 Jan 1;101(1):345–47. Epub 2002 Aug 8. PMID: 12393545. doi:10.1182/blood-2002-06-1851.
- Hantke J, Chandler D, King R, Wanders RJ, Angelicheva D, Tournev I, McNamara E, Kwa M, Guergueltcheva V, Kaneva R, et al. A mutation in an alternative untranslated exon of hexokinase I associated with hereditary motor and sensory neuropathy – russe (HMSNR). *Eur J Hum Genet.* 2009 Dec 17;17(12):1606–14. Epub 2009 Jun 17. PMID: 19536174; PMCID: PMC2987011. doi:10.1038/ejhg.2009.99.
- Sullivan LS, Koboldt DC, Bowne SJ, Lang S, Blanton SH, Cadena E, Avery CE, Lewis RA, Webb-Jones K, Wheaton DH, et al. A dominant

- mutation in hexokinase 1 (HK1) causes retinitis pigmentosa. *Invest Ophthalmol Vis Sci.* 2014 Sep 4;55(11):7147–58. PMID: 25190649; PMCID: PMC4224580. doi:10.1167/iops.14-15419.
10. Wang F, Wang Y, Zhang B, Zhao L, Lyubasyuk V, Wang K, Xu M, Li Y, Wu F, Wen C, et al. A missense mutation in HK1 leads to autosomal dominant retinitis pigmentosa. *Invest Ophthalmol Vis Sci.* 2014 Oct 14;55(11):7159–64. PMID: 25316723; PMCID: PMC4224578. doi:10.1167/iops.14-15520.
 11. Yuan Z, Li B, Xu M, Chang EY, Li H, Yang L, Wu S, Soens ZT, Y L, Wong LC, et al. The phenotypic variability of HK1-associated retinal dystrophy. *Sci Rep.* 2017 Aug 1;7(1):7051. PMID: 28765615; PMCID: PMC5539152. doi:10.1038/s41598-017-07629-3.
 12. Martin-Merida I, Aguilera-Garcia D, Fernandez-San Jose P, Blanco-Kelly F, Zurita O, Almoguera B, Garcia-Sandoval B, Avila-Fernandez A, Arteche A, Minguez P, et al. Toward the mutational landscape of autosomal dominant retinitis pigmentosa: a comprehensive analysis of 258 Spanish families. *Invest Ophthalmol Vis Sci.* 2018 May 1;59(6):2345–54. PMID: 29847639. doi:10.1167/iops.18-23854.
 13. Sato S, Morimoto T, Hotta K, Fujikado T, Nishida K. Eleven-year follow-up of a Japanese retinitis pigmentosa patient with an HK1 gene mutation. *Ophthalmic Genet.* 2019 Oct;40(5):466–69. Epub 2019 Oct 17. PMID: 31621442. doi:10.1080/13816810.2019.1678179.
 14. Okur V, Cho MT, van Wijk R, van Oirschot B, Picker J, Coury SA, Grange D, Manwaring L, Krantz I, Muraresku CC, et al. De novo variants in HK1 associated with neurodevelopmental abnormalities and visual impairment. *Eur J Hum Genet.* 2019 Jul;27(7):1081–89. Epub 2019 Feb 18. PMID: 30778173; PMCID: PMC6777464. doi:10.1038/s41431-019-0366-9
 15. McCulloch DL, Marmor MF, Brigell MG, Hamilton R, Holder GE, Tzekov R, Bach M. ISCEV Standard for full-field clinical electroretinography (2015 update). *Doc Ophthalmol.* 2015 Feb;130(1):1–12. Epub 2014 Dec 14. Erratum in: *Doc Ophthalmol.* 2015 Aug;131(1):81–3. PMID: 25502644. doi:10.1007/s10633-014-9473-7.
 16. Gocho K, Akeo K, Itoh N, Kameya S, Hayashi T, Katagiri S, Gekka T, Ohkuma Y, Tsuneoka H, Takahashi H. High-resolution adaptive optics retinal image analysis at early stage central areolar choroidal dystrophy with PRPH2 mutation. *Ophthalmic Surg Lasers Imaging Retina.* 2016 Dec 1;47(12):1115–26. PMID: 27977834. doi:10.3928/23258160-20161130-05.
 17. Feng S, Gale MJ, Fay JD, Faridi A, Titus HE, Garg AK, Michaels KV, Erker LR, Peters D, Smith TB, et al. Assessment of different sampling methods for measuring and representing macular cone density using flood-illuminated adaptive optics. *Invest Ophthalmol Vis Sci.* 2015 Sep;56(10):5751–63. PMID: 26325414; PMCID: PMC4559213. doi:10.1167/iops.15-16954.
 18. Li H, Durbin R. Fast and accurate long-read alignment with Burrows-Wheeler transform. *Bioinformatics.* 2010 Mar 1;26(5):589–95. Epub 2010 Jan 15. PMID: 20080505; PMCID: PMC2828108. doi:10.1093/bioinformatics/btp698.
 19. McKenna A, Hanna M, Banks E, Sivachenko A, Cibulskis K, Kernytsky A, Garimella K, Altshuler D, Gabriel S, Daly M, et al. The Genome Analysis Toolkit: a MapReduce framework for analyzing next-generation DNA sequencing data. *Genome Res.* 2010 Sep;20(9):1297–303. Epub 2010 Jul 19. PMID: 20644199; PMCID: PMC2928508. doi:10.1101/gr.107524.110
 20. Cingolani P, Platts A, Wang le L, Coon M, Nguyen T, Wang L, Land SJ, Lu X, Ruden DM. A program for annotating and predicting the effects of single nucleotide polymorphisms, SnpEff: sNPs in the genome of *Drosophila melanogaster* strain w1118; iso-2; iso-3. *Fly (Austin).* 2012 Apr-Jun;6(2):80–92. PMID: 22728672; PMCID: PMC3679285. doi:10.4161/fly.19695.
 21. Richards S, Aziz N, Bale S, Bick D, Das S, Gastier-Foster J, Grody WW, Hegde M, Lyon E, Spector E, et al. Standards and guidelines for the interpretation of sequence variants: a joint consensus recommendation of the American college of medical genetics and genomics and the association for molecular pathology. *Genet Med.* 2015 May 5;17(5):405–24. Epub 2015 Mar 5. PMID: 25741868; PMCID: PMC4544753. doi:10.1038/gim.2015.30.